



Petrological analysis of the pyroclastic and volcanic rocks in northwestern Mahneshan, northern Urmia-Dokhtar, NW Iran

Mojgan Salehi Yazdi ¹, Mansour Ghorbani ^{2,*}, Nima Nezafati ¹, Mansour Vossoughi Abedini ¹

¹ Department of Earth Sciences, Science and Research Branch, Islamic Azad University, Tehran, Iran

² Faculty of Earth Sciences, Shahid Beheshti University, Tehran, Iran

Received: 29 January 2020, Revised: 16 May 2020, Accepted: 20 June 2020

© University of Tehran

Abstract

The study area is a part of the northern Urmia-Dokhtar magmatic belt, which consists of andesite, basalt and acidic tuff. There are hyaloclastites with a clear bedding only in the NW part of Mahneshan area located in the northern Urmia-Dokhtar magmatic belt of Iran. In this region the volcanism commence during the Oligocene time with extremely strong hyaloclastite eruptions, and then after a pause, the volcanism continued by exceptionally extensive acidic tuff eruptions, and eventually ended up with the late Miocene basaltic andesite lava eruptions. Field observations, mineralogy and petrography on the major and minor minerals of the volcanic and sedimentary rocks indicate that three phases of volcanism occurred in the area. The hyaloclastites (Phase 1), are often composed of andesite and quartz-andesite to dacite. The highly extensive second phase consists of acidic tuffs interbedded with limestone. According to the fossil content and the ⁸⁷Sr/⁸⁶Sr age determination, this phase formed during the Chattian to Burdigalian ages. Phase 3 includes andesite-basalt, andesite and quartz-andesite. Based on the geochemical diagrams all three phases are situated within the calc-alkaline field, indicating the subduction of an oceanic crust under the continental crust.

Keywords: Petrogenesis, Hyaloclastites, ⁸⁷Sr/⁸⁶Sr Age Determination, Mahneshan.

Introduction

The study area is located in the northern Urmia-Dokhtar magmatic belt, NW Mahneshan, Zanjan City, which is part of Takab 1:250000 geological map (Alavi & Amidi, 1976) and Mahneshan-Takht-e Soleyman 1:100000 sheet (Ghahamghash & Babakhani, 1991; Lotfi, 2001) (Fig. 1). This area is distinguished from other parts of the Urmia-Dokhtar Magmatic belt based on two characteristics: 1) the presence of Precambrian basement which is overlain by the studied volcanic rocks; 2) the variations in the abundance of the Oligo-Miocene volcanic rocks. The Eocene volcanic rocks of the study area are very rare in comparison to those of other parts of Urmia-Dokhtar Magmatic belt. The main purpose of this study is to determine differences among the rock units, petrographical properties of the rock types, the age of the volcanic rocks, the petrogenesis, magmatic series and tectonic setting of the study area.

Many papers have been carried out on volcanic rocks of the area, however, the main concern was mineralization (e.g., Mehrabi et al., 1999; Asadi et al., 2000; Ojaghi, 2005; Daliran, 2008; Heidari, et al., 2015).

* Corresponding author e-mail: m-ghorbani@sbu.ac.ir

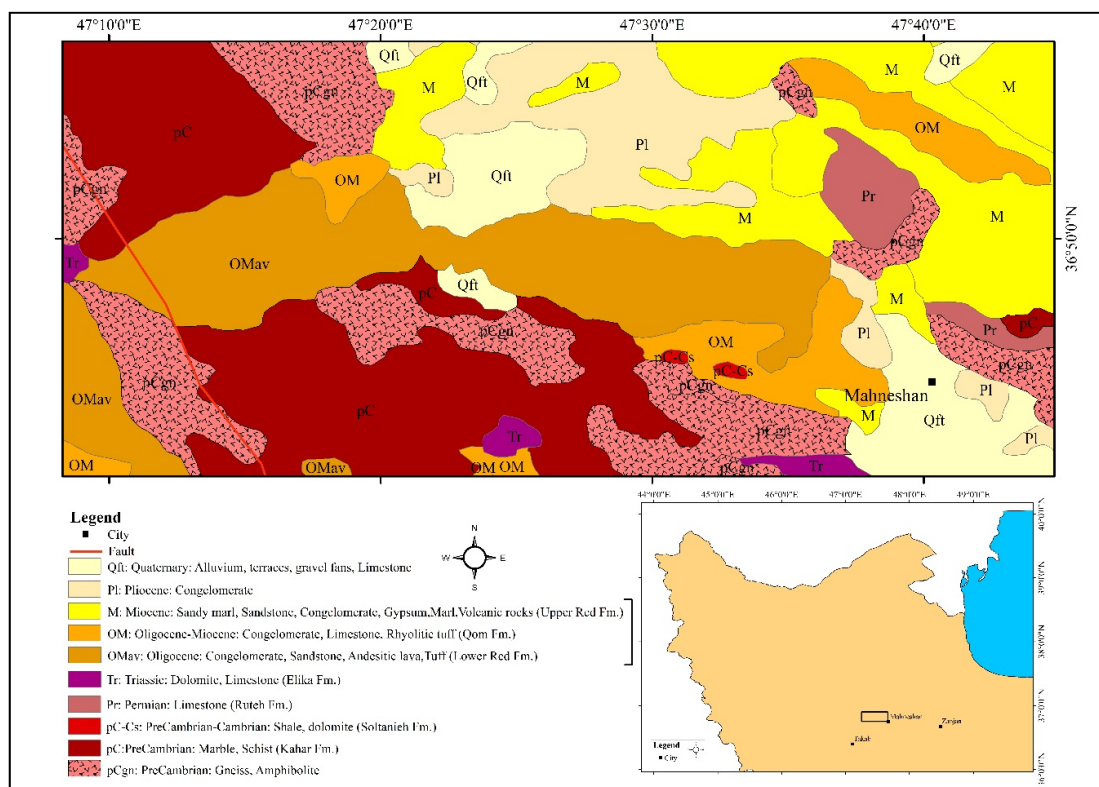


Figure 1. Geological map of the study area, Simplified and modified after Alavi & Amidi, 1976

Materials and Methods

The field observations and laboratory examinations have been carried out to reveal the geological relations among the basement, volcanic and associated rocks:

- Petrographical studies of 50 thin sections.
- Geochemical studies of 17 samples using ICP-MS method for trace elements as well as XRF for major elements at the Zarazma Mineral Studies Company.
- $^{87}\text{Sr}/^{86}\text{Sr}$ age determination and studying the fossil content of the limestones associated with the volcanic rocks: To determine the age of the limestone by strontium method, about 100 mg of rock powder was dissolved in %2.5 normal chloride acid. Then, strontium was isolated in a standard column containing resin, as defined by (Pin et al., 1994). Strontium isotopes were measured by the Triton plus Spectrometer at the center of Recherches Petrographiques et Geochimiques (CRPG-CNRS) in Nancy, France. During the experiment, the mass fractionation was normalized to an isotope ratio of $^{86}\text{Sr}/^{88}\text{Sr}$ of 0.1194.
- Chemo-mineral studies using EPMA by measuring 60 points on the plagioclase and pyroxene: To determine the thermobarometry of the plagioclase and pyroxene minerals, with an Electron Probe Micro Analyzer and an electron microprocessor, they were processed using SX100 model made by Cameca France, at the Minerals Processing Research Center of Iran. This device works with the KV15 accelerator voltage and nA20 current, and provides a detailed quantitative analysis with a resolution of 10 to 100 microns at any desired point from the element Beryllium (Be) to the uranium (U).

Discussion

From tectonics point of view, the study area is located in Central Iran, the northern Urmia-Dokhtar magmatic belt (Stocklin, 1968). The Central Iran is one of the major tectonic units of

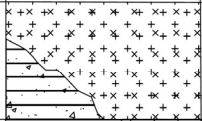
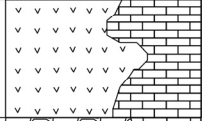
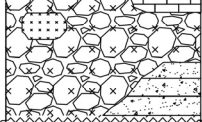
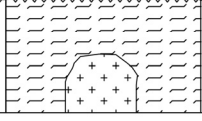
Iran, being amongst the most complex and largest geological units of the country (Ghorbani, 1999). It is situated between two main sutures of Paleo-Tethys in the north and Neo-Tethys in the south (Aghanabati, 2004). The Urmia-Dokhtar magmatic belt, constituting the western part of Central Iran, extends from northwest (Urmia or Sahand volcano) to southeast (Dokhtar a city near the Bazman volcano) (Berberian & King, 1981; Amidi et al., 1984; Emami, 1992). The Urmia-Dokhtar or Sahand-Bazman magmatic belt (Ghorbani, 2014) extends from the volcano of Sahand (NW Iran) in the northwest to the volcano of Bazman (SE Iran) in the southeast. This belt has a length of about 1500 km and an average width of about 80 km, where the study area is located in the northwestern part of this belt. There are alternation zones of sedimentary and volcanic sequences in this belt, most of them are composed of pyroclastic rocks. The sequence introduced by Amidi (1997) in Natanz-Surk; Emami (1991) in Qom; Jabari (2013) in Kashan-Zefreh and Dehlavi (1987) in Saveh but not in the same value. Many intrusive rocks (gabbro and granite) with the age of Eocene to Pliocene have intruded into Urmia-Dokhtar magmatic belt (Ghorbani, 2014). The Precambrian basements have been rarely reported in the southern part of this belt because of the huge value of volcanic rocks, while they have been reported in the northwestern part especially in the study area based on the geological maps of Takab 1:250000 (Alavi & Amidi, 1976) and Mahneshan 1:100000 (Lotfi, 2001). During the Cenozoic, volcanism in this belt experienced the activity peaks, including mid- and late Eocene, early and late Oligo-Miocene, early Miocene, and late Miocene-Pliocene (Emami, 1991; Ghorbani, 2014).

In the study area, the lithology from base to top is as follows (Figs. 3 and 4):

Phase1: The hyaloclastites are equivalent to lower red Formation. Considering the field studies, this phase encompasses the thickest unit of the volcanic rocks in the study area, but its distribution is only observed in the study area, and in other areas such as Urmia-Dokhtar magmatic belt and even in the northwestern Iran is invisible. Several characteristics might be mentioned on how these unique pyroclastic rocks originate; (1) These rocks are very diverse and have different volcanic components, and in Iran they are unique in this regard, and volcanic components in these units vary from ash to boulders, being more than several meters in diameter (Fig. 2a,b); (2) the rocks are erupted on the Precambrian metamorphic beds, which have a high thickness in the study area. (3) Rocks are erupted in a marine environment because of the fine particles (cement) and the petrographic studies of their coarse aggregates. (4) The geochemical and petrographic characteristics of the hyaloclastites show that they are differentiated from a more mafic magma. In addition, the field and petrographic evidence suggest a phreatomagmatic eruption for the rocks. (5) The topographic evidence of the area in the present time indicate a very submerged rough morphology and a horst-graben environment. However, the evidence, according to the paleogeographical studies (Ghorbani & Salehi, 2018), show that the Oligo-Miocene to Quaternary are much more evident than the present time.



Figure 2. a,b) Volcanic components of phase 1 (a: 47° 31'19"E, 36° 46'24"N and b: 47° 31'59"E, 36° 47'28"N) and c) Inter-fingering contact of phase 3 (47° 19'29"E, 36° 53'10"N)

Phase Type	Period/Epoch	Formation	Section		Lithology
			W	E	
Phase 3	Mid. and upper Miocene	Upper Red F.			Basalt and andesite Sandstone
Phase 2	Upper Oligocene-Lower Miocene	Equivalent Qom F.			Fossiliferous limestone Acidic tuff
Phase 1	Oligocene	Equivalent Lower Red F.			Limestone Andesitic mass Hyaloclastite Sandstone
	Precambrian				Pre. Basement Doran granite

	Shale		Sandstone		Andesitic mass		Acidic tuff
	Granite		Hyaloclastite		Limestone		Basalt and andesite

Figure 3. Lithological sequence of the study area



Figure 4. An image of the study area (47° 31'50"E, 36° 47'28"N)

Phase2: The acidic tuffs that are equivalent to lower parts of Qom formation, and they overlie the hyaloclastites (phase 1). The Qom formation limestone is placed between an acidic tuffs (phase 2) and upper part of hyaloclastites (phase 1). The tuffs replace a part of it or the whole of it. Based on the fossil content and the $^{87}\text{Sr}/^{86}\text{Sr}$ age determination, limestones indicate late Oligocene-early Miocene ages (Chatting-Burdigalian) that are in line with the zircon U-Pb age determination on Tuzlar volcanic rocks which is about 18.1 ± 1.0 to 19.3 ± 0.3 Ma. (Heidari et al., 2013, 2015), and the K/Ar and Ar/Ar age determinations on hydrothermal argillic alteration (whole rock and separated clay size fractions) and on volcanic rocks of Zarshuran indicate a 14.2 ± 0.4 Ma. (Mehrabi et al., 1999).

Phase 3: The volcanic lavas that are equivalent to upper red formation (with the age of mid-upper Miocene based on Figs. 3 and 4). After a break in the volcanic activity (dormant volcano) in the region, the evidence of which is the sedimentation of Aquitanian-Burdigalian rocks

(based on fossil evidence), a very strong volcanic phase began, which completely affected the study area. This phase can be traced out of the study area (according to field surveys). The rocks sometimes are of inter-fingering contact with the upper and middle parts of the Upper Red Formation, but gradually replace it (Fig. 2c). This is why we have given a middle-late Miocene age to volcanic rocks of phase 3 (Figs. 3 and 4).

Two fault groups have been determined in the study area; group I, the northwest-southeast trending faults that are older and occurred in Precambrian (Lotfi, 2001), and group II that are perpendicular to group I and affected the volcanic rocks and the Qom Formation (Ghahamghash & Babakhani, 1991; Lotfi, 2001). One example is the fault that passes through the Baichebagh mine and is perpendicular to the Qezelozan River (Ghorbani, 1999). The faults have been activated in the Cenozoic Era, especially in the Neogene, based on the geological maps of Takab 1:250000 (Alavi & Amidi, 1976), Mahneshan-Takht-e Soleyman 1:100000 (Ghahamghash & Babakhani, 1991; Lotfi, 2001) and the presence of volcanic rocks near these faults; (Ghorbani, 1999). The activity of the faults in the study area caused the creation of a horst-graben structure as the Qezelozan River passes through the graben block. The middle-late Miocene sedimentary rocks crop out in the surrounding areas of Qezelozan River. The horst is mainly covered with tuffs, hyaloclastites and andesite-basalts.

Petrography

The volcanic rocks of the study area, as mentioned above, are formed in three successive volcanic phases.

Phase 1: hyaloclastites: they consist of andesite and quartz-andesite to dacite. These rocks in hand specimens are of fine-grained texture and gray to brown in color. Their texture is often porphyroclastic with glassy and fine-grained matrix. Minerals that constitute the rocks have abundant plagioclase, resorbed biotite and pyroxene crystals that occupy rock texture. Plagioclase with polysynthetic twinning is present as phenocrysts and microlite. Based on extinction angle, plagioclase crystals are of andesine to labradorite type (Table 2). Pyroxene crystals are subhedral to anhedral, and are of the orthopyroxene and clinopyroxene types (Table 4; Sample M15). Quartz crystals, plagioclase and minor alkali feldspar have been distinguished on the basis of refractive index (Fig. 5a). Petrographic studies show a relative overlapping with rock chemistry studies and the norms, but sometimes in the quartz-andesites that are of the close composition to dacite, the quartz value calculated is more than 20%, but is not conformed in the mode.

Phase 2: Acidic Tuffs: these tuffs are of a white to green color in hand specimens. They are of volcanoclastic texture in microscopic samples and more than 30 percent of the rocks is composed of a glassy matrix and made of mostly quartz, broken plagioclase phenocrysts and occasionally alkali feldspar. Considering the components, they can be named as crystal- vitric acidic tuffs (Fig. 5b).

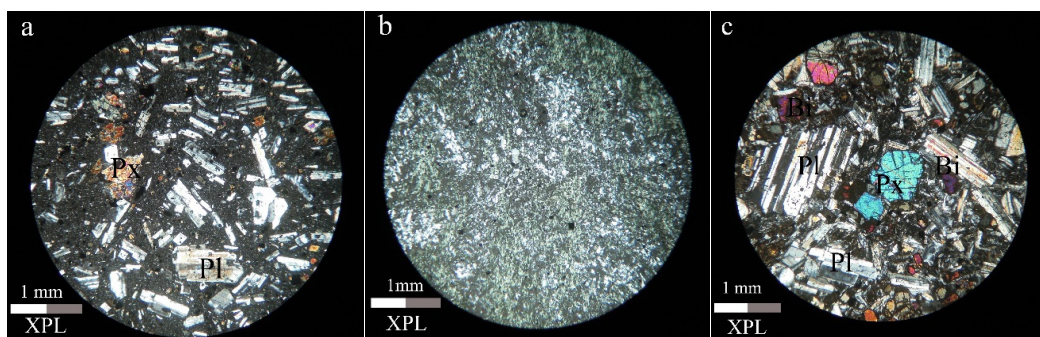


Figure 5. Microphotographs of phases 1, 2 and 3, respectively

Phase 3: volcanic lavas: they consist of basaltic andesite, andesite and quartz-andesite.

Basaltic andesite: in hand specimens, the andesite-basalts of the Mahneshan area are light grey in color and their plagioclases are of a white color. They are of porphyritic texture with a fine-grained glassy microlite matrix under polarizing microscope. The minerals are mainly composed of abundant plagioclase crystals with polysynthetic twinning, minor alkali feldspar, pyroxene as phenocryst and microlite which are decomposed in some samples. Based on extinction angle, plagioclase crystals are of Labradorite and Bytownite type and exhibit the same general trend from Ca to Na (Fig. 5c). The opaque minerals appear in euhedral forms. The zircon crystals are included in the plagioclase. Biotite crystals are of various sizes, which in most cases host the opaque minerals. In some samples of andesite-basalt, plagioclase crystals appear as phenocrysts and microlite, showing the ophitic and subophitic textures, which indicates a high volume of eruptions, and the formation of a large thickness of the rocks can be traced in the field studies. The euhedral pyroxenes are formed between the plagioclases. Alkali feldspar crystals are found to be low in rock matrix. Two types of plagioclases have been distinguished in the rock types. Some of them are unaltered and some altered. Few fractures of the rocks have been filled with calcite.

Andesite: In hand specimens, the rocks are generally dark gray to bright in color and have an ophitic to porphyritic textures with a microlitic matrix. The main mineral is plagioclase crystals with sometimes crossed structure aggregate. Plagioclases are observed in both microlite and phenocryst forms with polysynthetic twinning. In some rocks, the plagioclase crystals have been altered into sericite – and carbonates. Alkali feldspar crystals constitute less than 10% of the matrix. There are two types of plagioclases in the rocks. Some are intact, and some have been decomposed, containing opaque minerals. Based on the extinction angle, the plagioclase is of andesine-labradorite type. The euhedral pyroxene crystals occupy the space between the plagioclases. In petrographic studies, the values of plagioclase phenocrysts (20-30%) and pyroxene (8%) have been estimated. In these rocks, there are often fractures that are filled with calcite, and sometimes the hornblende is abundant enough to name it hornblende-andesite.

Quartz-andesite: Based on petrographic studies carried out on the selected samples, they represent quartz-andesite composition. The rocks are of porphyritic texture with a glassy matrix. More than 65% of the constituents of the rocks are composed of plagioclase crystals as phenocryst and microlite. Quartz crystals are more than 5 percent in the form of phenocryst. Alkali feldspar crystals are found to be low in matrix, about 10-25%. Biotite crystals are mostly observed as phenocrysts and less as microlite. Pyroxene crystals can be seen as phenocrysts, which are more abundant in andesite-basalt and significantly reduce in quartz-andesites. Sometimes, when the amount of quartz and alkali feldspar increases, sanidine can be seen, which can imply dacite is also found.

Age determination

We have chosen three samples of acidic tuffs interbedded with limestones from Qezelozan river (Baghcheh mine) (Q3, Q5 and Q25).

Ages were estimated by comparison of the measured $^{87}\text{Sr}/^{86}\text{Sr}$ ratios with the established seawater evolution curve (Prokoph et al., 2008). Age ranges given below include uncertainties on both the measured $^{87}\text{Sr}/^{86}\text{Sr}$ ratios and the marine Sr isotope curve. Comparing paleontological ages are based on International Chronostratigraphic Chart (Cohen et al., 2020). Samples Q3 and Q5 display indiscernible $^{87}\text{Sr}/^{86}\text{Sr}$ isotopic ratios (0.708274 and 0.708298, respectively), corresponding to an age range of 22 to 25 Ma. Sample Q25 has a slightly higher $^{87}\text{Sr}/^{86}\text{Sr}$ ratio (0.708350), corresponding to an age range of 21 to 23 Ma. The Sr age determination of sample Q3 is consistent with the Aquitanian age determined by the fossil content. For samples Q5 and Q25, the data yielded an age slightly older than the Burdigalian

time determined by the microfossils, assuming an age range of 16.0 to 20.4 Ma. for the Burdigalian time period (Table 1).

Mineral Chemistry

After field and microscopic examinations, in order to access the chemical composition of minerals from thin-sections of phases 1 and 3, 3 fresh and least-altered samples of andesite and basaltic andesite rocks, were selected for microprobe test. The results are presented in tables 2 to 5.

Table 1. Microfossils identified in limestones of phase 2

Sample No.	microfossil	Age
Q3	<i>Kuphus arenarius</i> , <i>Pseudolituonella reicheli</i> , <i>Asterigerina rotula</i> , <i>Dendritina</i> cf. <i>Rangi</i> , <i>Archaias kirkukensis</i> , <i>Textularia</i> sp., <i>Miogypsina</i> sp., <i>Amphistegina</i> sp., <i>Echinoid</i> sp.3, <i>Echinoid</i> spine, Echinoid fragments, Peneroplids, Gastropods, abundant Miliolids, <i>Lithophyllum</i> sp., <i>Archeolithothamnium</i> sp., Echinoid And other Algal fragments	Miocene (Aquitainian)
Q5	<i>Globigerinoides</i> cf. <i>diminutus</i> , <i>Globigerinoides immaturus</i> , <i>Amphistegina</i> sp., <i>Miogypsina</i> sp., <i>Globigerinoides</i> cf. <i>subquadratus</i> , <i>Eulepidina dilitata</i> , <i>Kuphus arenarius</i> , <i>Solenomeris ogermani</i> , <i>Globigerinoides</i> cf. <i>Altiapertura</i> , <i>Textularia</i> sp., <i>Echinoid</i> sp.3, <i>Lepidocyclina</i> sp., coral, <i>Echinoid</i> spine, <i>Echinoid</i> fragments, <i>Globigerinids</i> , <i>Dacycladaceans</i> , Shell and <i>Bryozoa</i> fragments.	Miocene (Burdigalian)
Q25	<i>Globigerinoides diminutus</i> , <i>Globigerinoides subquadratus</i> , <i>Pseudolituonella reicheli</i> , <i>Operculina complanata</i> , <i>Miogypsina</i> sp., <i>Amphistegina</i> sp., <i>Elphidium</i> sp., <i>Cibicides</i> sp., <i>Lenticulina</i> sp., <i>Bigenarina</i> sp., <i>Nodosaria</i> sp., <i>Textularia</i> sp., <i>Operculina</i> sp., <i>Bryozoa</i> fragments, <i>Echinoid</i> fragments, Shell and Algal fragments.	Miocene (Burdigalian)

Table 2. Results of electron microprobe analysis of Plagioclase in phase 1 (wt.%) (Structural Formula Based on Oxygen 8)

Sample No.	M15-33 (Core)	M15-34 (Rim)	M15-40	M15-49	M15-59	M15-60
Phase type	Phase 1					
SiO ₂	58.72	54.27	53.28	55.54	57.67	52.88
TiO ₂	0.06	0	0.03	0.02	0.03	0.03
Al ₂ O ₃	24.87	28.92	28.29	27.83	25.47	28.8
Cr ₂ O ₃	0	0	0.04	0	0	0.02
FeO	0	0	0.17	0	0	0.41
MgO	0.02	0.01	0.03	0.04	0.07	0.16
CaO	8.43	11.6	11.69	10.87	8.77	11.83
Na ₂ O	6.44	4.68	4.99	5.21	6.48	3.49
K ₂ O	0.53	0.33	0.27	0.08	0.54	0.92
Total	99.9	99.89	98.82	99.6	99.04	98.55
Si	2.65	2.46	2.45	2.51	2.62	2.44
Ti	0	0	0	0	0	0
Al	1.32	1.54	1.53	1.48	1.36	1.57
Cr	0	0	0	0	0	0
Fe	0	0	0.01	0	0	0.02
Mn	0	0	0	0	0	0
Mg	0.001	0	0	0	0	0.01
Ca	0.40	0.56	0.58	0.53	0.43	0.58

Na		0.56	0.41	0.44	0.46	0.57	0.31
K		0.031	0.02	0.02	0	0.03	0.05
X An		40.695	56.69	60.07	53.3	41.49	61.48
X Ab		56.25	41.38	38.32	46.23	55.47	32.82
X Or		3.04	1.92	1.6	0.47	3.04	5.69
Plagioclase Type		Andesine	Labradorite	Labradorite	Labradorite	Andesine	Labradorite
Putirka	T(C)	1063.6	1060.9	1059	1084.9	1075.7	1090.5
(2005) Eqn 23	T(C) sat	1045.2	1032.3	1032.3	1052.9	1052.9	1045.2
Eqn (24a)	T(C)	1074.7	1070.3	1067.8	1103.8	1091.4	1110.4
Eqn (25b)	H₂O (wt. %)	0.3	0.6	0.7	0.6	1.1	0.2
Eqn (25a)	P(kbar)	4.2	0.2	0.3	1.4	4.3	0.5
Eqn 26	T(C) sat	1098.2	1073.2	1073.2	1113.2	1113.2	1098.2
Observed	K_D (Ab-An)	0.23	0.12	0.13	0.15	0.23	0.09

Table 3. Results of electron microprobe analysis of Plagioclase in phase 3 (wt.%) (Structural Formula Based on Oxygen 8)

Sample No.	M35-1 (Core)	M35-4 (Rim)	M35-12	M35-14	M35-21	M35-23	M35-25	M35-30
Phase type	Phase 3							
SiO₂	52.63	53.42	49.13	54.83	51.54	48.88	54.32	49.88
TiO₂	0.08	0.18	0.4	0.22	0.36	0.03	0.06	0.02
Al₂O₃	28.99	28.11	30.5	26.55	1.23	30.81	27.59	31.59
Cr₂O₃	0	0	0.04	0	0.05	0.05	0.09	0.04
FeO	0.16	0.69	0.73	0.64	18.53	0.4	0.74	0
MgO	0.09	0.13	0.08	0.08	23.75	0.09	0.12	0.1
CaO	12.4	11.81	15.8	10.97	1.85	16.44	12.05	15.51
Na₂O	3.97	4.58	2.23	5.33	0.08	1.76	3.69	2.25
K₂O	0.55	0.36	0.15	0.43	0.18	0.55	0.45	0.13
Total	98.91	99.32	99.08	99.08	98.03	99.03	99.15	99.54
Si	2.42	2.45	2.28	2.52	2.42	2.27	2.51	2.3
Ti	0	0	0.01	0.01	0.01	0	0	0
Al	1.57	1.52	1.67	1.44	0.07	1.69	1.5	1.71
Cr	0	0	0	0	0	0	0	0
Fe	0.01	0.03	0.03	0.02	0.08	0.02	0.29	0
Mn	0	0	0	0	0.02	0	0	0
Mg	0.01	0.01	0.01	0.01	1.79	0.01	0.01	0.01
Ca	0.61	0.58	0.79	0.54	0.1	0.82	0.6	0.76
Na	0.35	0.41	0.2	0.47	0.01	0.16	0.16	0.2
K	0.03	0.02	0.01	0.03	0.01	0.03	0.03	0.01
X An	61.27	57.53	78.94	51.92	83.74	81.07	62.55	78.59
X Ab	35.5	40.38	20.16	45.65	6.55	15.7	34.66	20.63
X Or	3.23	2.09	0.89	2.42	9.7	3.23	2.78	0.78
Plagioclase Type	Labradorite	Labradorite	Bytownite	Labradorite	Bytownite	Bytownite	Labradorite	Bytownite
Putirka	T(C)	1200.2	1194	1208.7	1172.1	1198.8	1184.7	1174.2
(2005) Eqn 23	T(C) sat	1169.5	1169.5	1169.5	1158.7	1158.7	1151.6	1151.6
Eqn (24a)	T(C)	1206.5	1198.4	1217.9	1169.2	1204.1	1185.1	1171.3
Eqn (25b)	H₂O (wt. %)	0	0.1	0.2	0.5	0.4	0.4	0.4
Eqn (25a)	P(kbar)	7	7.5	4.3	8.1	5.9	3.9	3.7
Eqn 26	T(C) sat	1194.1	1194.1	1194.1	1174	1174	1161	1161
Observed	K_D (Ab-An)	0.25	0.3	0.11	0.38	0.03	0.08	0.11

Table 4. Results of electron microprobe analysis of pyroxene in phase 1 (wt.%) (Structural formula based on 6 oxygen atoms)

Sample No.	M15-37	M15-43	M15-44	M15-45	M15-47	M15-48	M15-50	M15-54	M15-55	M15-56	M15-57	M15-58
Phase Type	Phase 1											
SiO2	48.94	52.36	52.85	52.7	52.1	52.7	52.64	52.6	51.73	52.31	52.1	52.99
TiO2	0.58	0.11	0.19	0.1	0.11	0.23	0.13	0.11	0.13	0.09	0.16	0.12
Al2O3	2.41	0.37	0.95	0.42	0.45	0.86	0.46	0.33	0.35	0.33	0.65	0.35
Cr2O3	0	0	0	0.04	0	0	0	0	0	0	0	0
FeO	8.62	18.45	17.03	18	18.7	19.1	18.63	19.7	18.81	19.93	18.5	18.71
Mno	0.44	1.49	0	1.23	1.18	0.46	0.64	0	1.29	0.6	1.62	0.41
MgO	13.97	24.55	26.09	24.7	24.3	24.2	24.76	24.7	24.77	24.41	24.8	25.13
CaO	20.26	0.75	1.55	0.88	0.81	1.25	0.87	0.97	0.98	0.68	0.71	0.67
Na2O	0.36	0	0	0	0.03	0.02	0.03	0.05	0.05	0.05	0.08	0.06
K2O	0.02	0	0	0	1.16	0.01	0	0	0	0	0	0.01
Total	98.62	98.08	98.67	98.1	98.7	98.8	98.18	98.5	98.14	98.4	98.6	98.47
Si	1.913	1.958	1.941	1.97	1.96	1.95	1.962	1.95	1.93	1.953	1.94	1.967
Ti	0.017	0.003	0.005	0.03	0	0.01	0.004	0	0.004	0.003	0	0.003
Al	0.111	0.016	0.041	0.02	0.02	0.04	0.02	0.01	0.015	0.015	0.03	0.015
Cr	0	0	0	0	0	0	0	0	0	0	0	0
Fe3	0.085	0.062	0.066	0.04	0.06	0.06	0.05	0.88	0.118	0.079	0.1	0.049
Fe2	0.195	0.515	0.457	0.52	0.53	0.53	0.531	0.52	0.469	0.543	0.48	0.531
Mn	0.015	0.047	0	0.04	0.04	0.04	0.02	0.02	0.041	0.019	0.05	0.013
Mg	0.81	1.37	1.43	1.38	1.36	1.33	1.38	1.36	1.38	1.36	1.37	1.39
Ca	0.849	0.03	0.061	0.04	0.03	0.05	0.035	0.04	0.039	0.027	0.03	0.27
Na	0.027	0	0	0	0	0	0.002	0	0.004	0.004	0.01	0.004
Wo	43.64	1.52	3.03	1.78	1.65	2.51	1.74	1.91	1.96	1.35	1.43	1.33
En	41.87	69.27	70.98	69.78	68.73	67.59	69.09	67.72	68.76	67.66	69.51	69.60
Fs	14.49	29.21	25.99	28.43	29.62	29.90	29.16	30.37	29.29	30.99	29.05	29.07
Pyroxene Type	diopside	enstatite										

Table 5. Results of electron microprobe analysis of pyroxene in phase 3 (wt.%) (Structural formula based on 6 oxygen atoms)

Sample No.	M35-5	M35-6	M35-7	M35-8	M35-9	M-3515	M35-16	M35-17	M35-18	M35-19	M35-20
Phase Type	Phase 3										
SiO2	51.25	49.77	49.5	49.4	51.5	52.3	51.6	50.39	51.43	51.1	49.45
TiO2	0.54	0.61	0.67	1.21	0.41	0.28	0.78	0.23	2.39	0.34	0.74
Al2O3	2.02	1.78	1.99	1.71	1	0.28	1	0.86	1.06	1.11	1.44
Cr2O3	0.28	0	0	0	0	0.07	0	0.09	0.05	0.09	0.09
FeO	9.29	11.7	10.9	12.4	19.2	18.36	19.3	18.95	17.96	17.9	17.48
Mno	0.27	0.34	0.29	0.32	0.44	0.4	0.46	0.46	0.43	0.41	0.17
MgO	15.81	14.84	15.7	15.4	23.2	24.2	23.5	22.17	24.26	25.3	25.32
CaO	19.87	18.80	19	17.9	1.96	1.58	1.8	1.88	1.66	1.76	2.93
Na2O	0.30	0.26	0.32	0.22	0.06	0	0	0.09	0.06	0.16	0.24
K2O	0	0	0	0	0.17	0.1	0	3.17	0.02	0.1	0.19
Total	99.72	98.24	98.5	98.8	98	98.46	98.5	98.3	99.38	98.3	98.16
Si	1.90	1.89	1.87	1.87	1.94	1.967	1.93	1.958	1.908	1.89	1.833
Ti	0.02	0.02	0.02	0.03	0.01	0.008	0.02	0.007	0.067	0.01	0.021
Al	0.09	0.08	0.09	0.08	0.04	0.012	0.04	0.039	0.046	0.05	0.063
Cr	0.01	0.00	0	0	0	0.002	0	0.003	0.001	0	0.003
Fe3	0.01	0.12	0.16	0.13	0.06	0.036	0.05	0.029	0.004	0.16	0.244
Fe2	0.20	0.25	0.18	0.26	0.55	0.542	0.56	0.587	0.553	0.4	0.298
Mn	0.01	0.01	0.01	0.01	0.01	0.013	0.02	0.015	0.014	0.01	0.005

Mg	0.88	0.84	0.88	0.87	1.30	1.36	1.31	1.28	1.34	1.40	1.40
Ca	0.79	0.77	0.77	0.73	0.08	0.064	0.07	0.078	0.066	0.07	0.116
Na	0.02	0.02	0.02	1.02	0	0	0	0.007	0.004	0.01	0.017
Wo	40.45	38.70	38.5	36.6	3.98	3.19	3.63	3.96	3.36	3.45	5.66
En	44.78	42.50	44.28	43.68	65.57	67.91	66.03	64.92	68.28	69.06	68.01
Fs	14.76	18.80	17.26	19.75	30.45	28.90	30.34	31.13	28.36	27.48	26.34
Pyroxene Type	augite	augite	augite	augite	enstatite	enstatite	enstatite	enstatite	enstatite	enstatite	pigeonite

Table 5. (continued).

Sample No.	M35-21	M35-22	M35-28	M35-29	M35-68	M35-68	M35-69	M35-70	M35-71	M35-75	M35-76
Phase Type	Phase 3										
SiO₂	51.54	50.46	51.69	51.72	50.77	52.43	51.68	49.77	50.36	50.02	49.63
TiO₂	0.36	2.8	0.72	0.27	0.38	0.32	0.89	0.8	0.71	0.7	0.77
Al₂O₃	1.23	1.05	1.04	0.82	1.3	1.13	2.59	2.13	2.1	2	1.95
Cr₂O₃	0.05	0.06	0.04	0.02	0	0	0	0	0	0	0
FeO	18.53	18.17	18.66	18.77	21.68	19.73	8.11	10.87	10.86	10.71	10.81
MnO	0.4	0.47	0.29	0.46	0.43	0.4	0.32	0.3	0.34	0.28	0.3
MgO	23.75	24.11	22.87	22.94	22.92	23.52	15.5	15.18	15.28	16.03	15.58
CaO	1.85	1.71	1.91	1.66	2.85	2.9	20.44	18.46	19.83	20.26	20.15
Na₂O	0.08	0.17	0.05	0.08	0.03	0.1	0.32	0.29	0.28	0.4	0.29
K₂O	0.18	0.29	0	0	0.02	0.05	0.01	0.09	0.06	0.13	0.09
Total	98.03	99.29	97.35	96.74	100.51	100.8	100.03	98.12	99.95	100.96	99.92
Si	1.933	1.877	1.958	1.968	1.874	1.92	1.913	1.892	1.877	1.844	1.852
Ti	0.01	0.078	0.021	0.008	0.011	0.009	0.025	0.023	0.02	0.019	0.022
Al	0.054	0.046	0.046	0.037	0.057	0.49	0.113	0.095	0.092	0.087	0.086
Cr	0.001	0.002	0.001	0.001	0	0	0	0	0	0	0
Fe₃	0.65	0.054	0.591	0.017	0.176	0.1	0.035	0.095	0.134	0.214	0.188
Fe₂	0.516	0.511	0.009	0.58	0.493	0.505	0.216	0.25	0.205	0.116	0.15
Mn	0.013	0.015	1.292	0.015	0.013	0.012	0.01	0.01	0.011	0.009	0.009
Mg	1.33	1.34	0.08	1.30	1.26	1.28	0.89	0.86	0.85	0.88	0.87
Ca	0.074	0.068	0.004	0.068	0.113	0.114	0.81	0.752	0.792	0.8	0.806
Na	0.006	0.012	0.004	0.006	0.002	0.007	0.023	0.021	0.02	0.029	0.021
Wo	3.75	3.46	3.95	3.44	5.52	5.68	42.29	38.41	40.01	39.78	40.09
En	66.95	67.85	65.89	66.18	61.73	64.14	44.62	43.94	42.89	43.80	43.13
Fs	29.30	28.69	30.16	30.38	32.76	30.18	13.10	17.65	17.10	16.42	16.79
Pyroxene Type	enstatite	enstatite	enstatite	enstatite	pigeonite	pigeonite	augite	augite	augite	augite	augite

Chemistry of Plagioclase

Fig.6 is a plot of Plagioclases of volcanic rocks of phase 1 and 3 in the triangular graph of orthoclase-albite-anorthite. It is used to distinguish and classify the plagioclases of the study area. In this figure it can be seen that the plagioclases of phase 1 are located in two field of andesine and labradorite, and those of phase 3 are located in three field of labradorite, bytownite and anorthite. Therefore, the chemical composition of plagioclases indicates phase 1 lies in the andesite range, and phase 3 in the range of andesite-basalt. The petrographic evidence confirm the results.

Plagioclase thermobarometry

Plagioclase thermometry of andesite and basaltic andesite rocks from phases 1 and 3 based on Putirka (2008) is estimated about 1070°C to 1110°C and 1169°C to 1217°C, respectively. Phase 1 barometry based on Putirka (2008) is about 4 Kbar with KD: 0.12 to 0.23 and in phase 3 is at least 3.7 to 8 Kbar with KD: 0.3 to 0.25 that generally show low temperatures (Tables 2 and 3).

Comparison of andesite and basaltic andesite samples from phase 1 (M15-33 and M15-34)(Fig. 7a) and phase 3 (M35-1 and M35-4)(Fig. 7b) based on BSE images exhibit the same general trend from core to rim.

Chemistry of Pyroxene

The chemistry of the pyroxenes of the study area was studied on the andesite and basaltic andesite rocks of phases 1 and 3 and, as it is shown in the Wo–En–Fs diagram for pyroxenes (Morimoto, 1989), the pyroxenes of phases 1 and 3 are located within the range of Diopside, Augite, Pigeonite and Enstatite that represent andesite to andesite-basaltic compounds (Fig. 8a; Tables 4 and 5).

In diagram (Fig. 8b), pyroxenes are divided into four groups (1): Ca-Mg-Fe pyroxenes (Quad), 2) Ca-Na pyroxenes, 3) Na pyroxenes and 4) Other pyroxenes (Morimoto, 1989). The pyroxenes of phases 1 and 3 are located within the range of Ca-Mg-Fe. In this chart, the J and Q indices are calculated according to the following equations:

$$Q = Ca + Mg + Fe + 2 \text{ and } J = 2Na \pm R \pm (R: Al, Fe^{+3}, Cr^{+3}, Sc^{+3})$$

The Al_2O_3 diagram, against the SiO_2 shows the samples of Phases 1 and 3 are placed within the field of sub-alkaline and calc-alkaline basalts (Le Bas, 1962) (Fig. 8c).

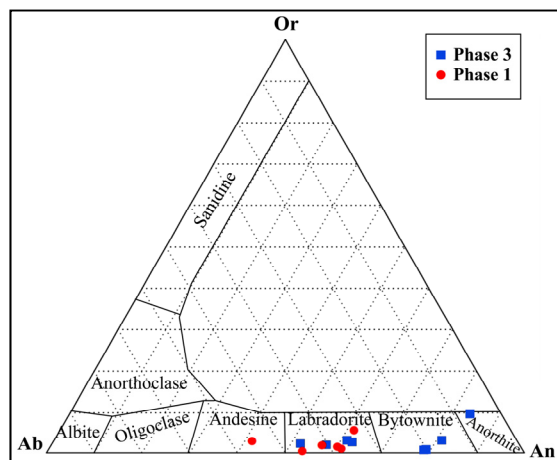


Figure 6. Plagioclases of volcanic rocks of phase 1 and 3 in the triangular graph of orthoclase-albite-anorthite

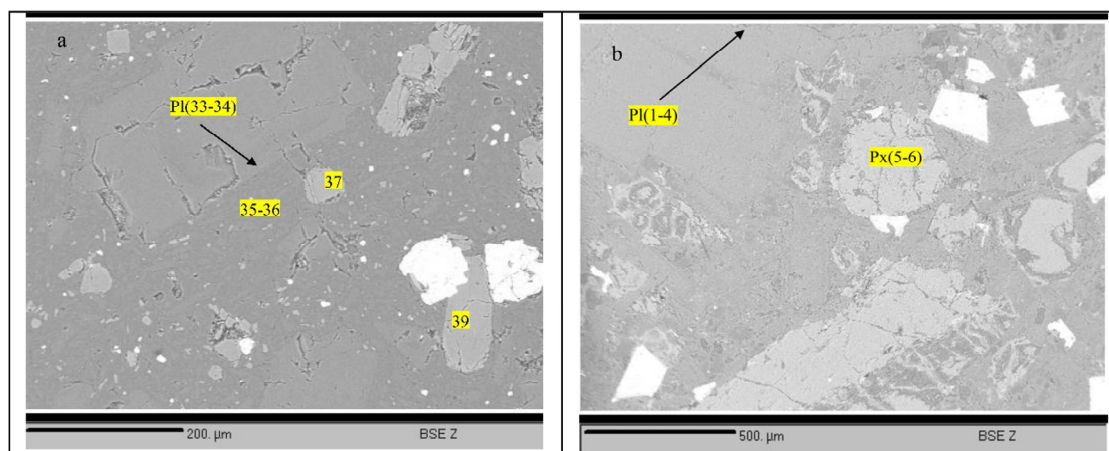


Figure 7. a, b) Analysis of Backscattered Scanning Electron microscope Images (BSEI) of thin sections from phases 1 and 3, respectively

Clinopyroxene thermobarometry

Clinopyroxenes thermobarometry of phases 1 and 3 based on the diagram Soesoo (1997) is estimated about 2 to 5 kbar (Fig. 9a) and 1100°C to 1150°C (Fig. 9b), indicating clinopyroxenes crystallization of the two phases are low and they all have been formed in a shallow depth that conform by presence of related mineral parageneses, consisting of quartz (phase1), alkali feldspar and pyroxene (phases 1 and 3) based on petrographic studies on Fig. 5.

Clinopyroxenes thermobarometry of basaltic andesite rocks from phases 1 and 3 based on Putirka (2008) equation (32d) give 0.1 to 4.6 Kbar pressure and 1053°C to 1077°C temperature and 3 Kbar pressure and 1079°C to 1145°C temperature, respectively (Table 6).

Table 6. The table of clinopyroxenes thermobarometry (Putirka, 2008)

Phase Type	Putirka <i>et al.</i> 1996	Putirka <i>et al.</i> 2003	Putirka 2008	Putirka 2008	Putirka 2008
	T(C)	T(C)	Eqn. 32c P(Kbar)	Eqn. 32d T(c)	Eqn. 35
Phase 1	1080.7	1079.7	4.6	1053.5	0.252
Phase 1	1057.4	1066.0	3.3	1077.8	0.252
Phase 3	1052.7	1055.2	0.1	1079.1	0.248
Phase 3	1119.6	1100.2	3.5	1145.7	0.262

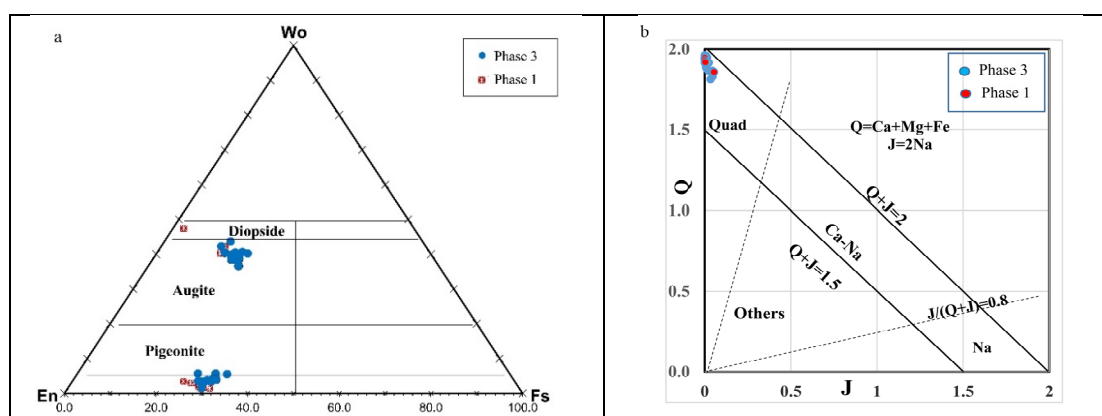


Figure 8. a) Diagram of phase 1 and phase 3 pyroxenes according to Wo-En-Fs (after Morimoto, 1989). b) Diagram of pyroxene classification based on the diagram J-Q (Morimoto, 1989). c) Diagram of magmatic series based on the diagram Al_2O_3/SiO_2 (Le Bas, 1962)

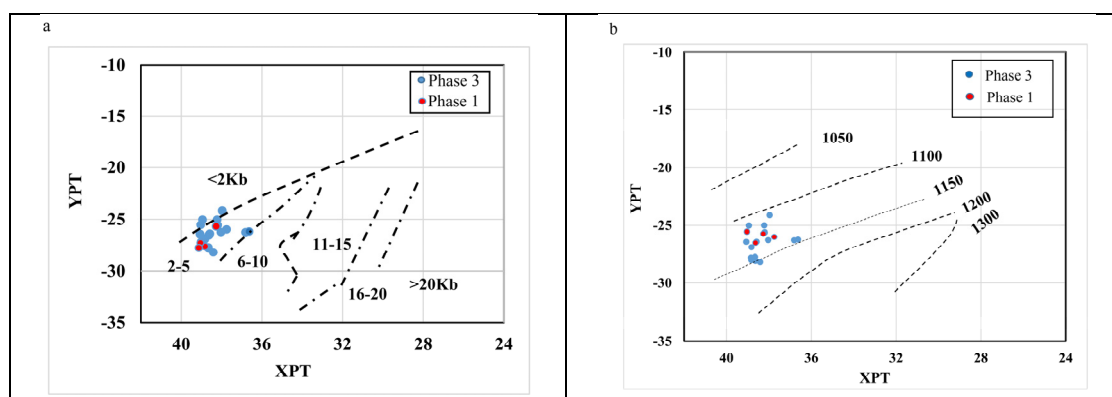


Figure 9. a) and b) Characterization diagram of Clinopyroxene crystallization of volcanic rocks from phases 1 and 3 based on the diagram Soesoo (1997). (XPT=0.446 SiO_2 + 0.187 TiO_2 -0.404 Al_2O_3 + 0.346 $FeO(t)$ - 0.052 MnO + 0.309 MgO + 0.431 CaO - 0.446 Na_2O . YPT= 0.369 SiO_2 + 0.535 TiO_2 - 0.317 Al_2O_3 + 0.323 $FeO(t)$ + 0.235 MnO - 0.516 MgO - 0.167 CaO - 0.153 Na_2O)

Whole-rock chemistry

For whole-rock major elements according to the diagram (Middlemost, 1985), by studying the chemistry of 17 samples collected from the three phases of the study area show the samples of phase 1 are located within the field of dacite, phase 2 within the field of andesite to dacite and phases 3 within the field of andesite-basalt and andesite (tables 7 and 8; Fig. 10).

Petrogenesis of the Mahneshan volcanic rocks

Based on the data, especially geochemical studies, the three volcanic phases show a magmatic geochemical affinity with each other and they all show a tendency to the calc-alkaline series that conform to Urmia- Dokhtar magmatic series (Fig. 11a).

Table 7. Whole rocks major elements (wt.%) composition of the Mahneshan area

Samples	SiO ₂	TiO ₂	Al ₂ O ₃	FeO	Fe ₂ O ₃	MnO	MgO	CaO	Na ₂ O	K ₂ O	P ₂ O ₅
M-2	67.90	0.33	14.5	0	0.00	-	5.21	1.16	0.29	3.50	0.11
M-5	57.39	0.75	15.47	5.04	6.72	0.06	4.28	6.60	3.05	2.38	0.22
M-7	60.87	0.07	16.38	3.89	0.78	-	1.52	7.20	3.98	2.07	0.17
M-8	63.68	0.76	15.21	2.87	0.70	0.05	0.63	6.68	4.14	2.73	0.19
M-9	62.98	0.55	14.77	4.06	0.89	0.05	1.33	6.11	3.8	3.00	0.19
M-12	61.83	0.55	14.4	5.47	1.17	-	3.50	4.86	2.88	2.94	0.15
M-13	68.14	0.41	13.31	3.01	0.66	-	3.23	3.53	1.64	4.73	0.09
M-14	70.82	0.44	12.06	3.67	0.80	-	1.74	3.67	2.18	2.06	0.10
M-15	66.55	0.60	11.58	4.75	1.04	0.13	2.77	5.65	3.8	1.57	0.19
M-16	62.26	0.58	14.95	5.34	1.15	0.13	2.66	5.58	3.7	1.64	-
M-20	62.01	0.60	13.82	5.39	1.16	0.12	2.67	5.94	3.84	1.63	0.19
M-21	62.08	0.60	14.5	5.69	1.22	0.14	2.70	5.59	3.73	1.66	0.18
M-25	62.18	0.70	13.52	5.51	1.20	0.12	3.15	6.65	3.32	1.81	0.15
M-26	59.66	0.67	15.9	5.14	1.13	0.11	3.02	6.43	3.413	1.78	0.14
M-30	66.02	0.59	11.92	4.38	0.96	-	1.61	5.84	2.95	3.16	0.12
M-35	58.95	0.89	15.26	5.71	1.28	0.16	2.60	7.54	2.93	2.25	0.16
M-38	68.40	0.50	13.87	3.04	0.68	-	0.45	5.19	3.5	2.69	0.16

Table 8. Whole rocks trace elements (ppm) composition of the Mahneshan area

Samples	S	Ba	Rb	La	Zr	Nb	Ni	Co	Zn	Cr	Ce	Pr
M-2	0.09	89	62	28	12	20.6	15	6.6	12	7	49	5.01
M-5	0.07	0.11	49	60	33	23.8	27	19.3	33	42	114	10.8
M-7	0.07	518	43	19	33	17.9	12	12.5	33	8	43	3.95
M-8	-	541	65	18	50	17.1	11	5.8	50	37	43	4.16
M-9	-	674	56	25	33	24.7	9	13.2	33	5	57	5.26
M-12	-	413	54	21	21	22.4	10	11.2	21	5	49	5.29
M-13	-	541	97	17	8	17.2	13	5.4	8	7	34	4.14
M-14	-	338	40	27	16	15.9	9	7.8	16	7	52	5.36
M-15	-	538	37	23	50	22.7	6	12.1	50	8	51	5.07
M-16	0.18	569	38	25	51	26.6	5	11.9	51	14	55	5.47
M-20	-	586	50	24	53	25.4	4	12	53	9	53	7.3
M-21	-	656	45	24	82	21.9	12	13.5	82	9	49	5.01
M-25	0.06	446	45	18	46	20.1	11	13.8	46	9	114	10.8
M-26	-	497	50	22	46	16.7	7	15.4	46	9	43	3.95
M-30	-	520	72	15	100	16.9	11	10.6	100	22	43	4.16
M-35	0.09	412	67	20	56	18.3	27	17.6	56	59	57	5.26
M-38	0.16	621	75	23	37	22.1	7	5.5	37	12	49	5.29

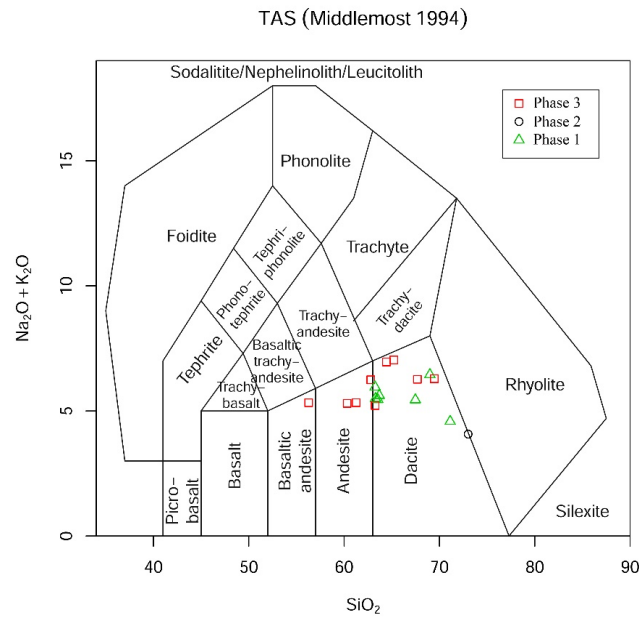


Figure 10. Classification of volcanic rocks in the study area based on the T.A.S chart (Middlemost, 1994)

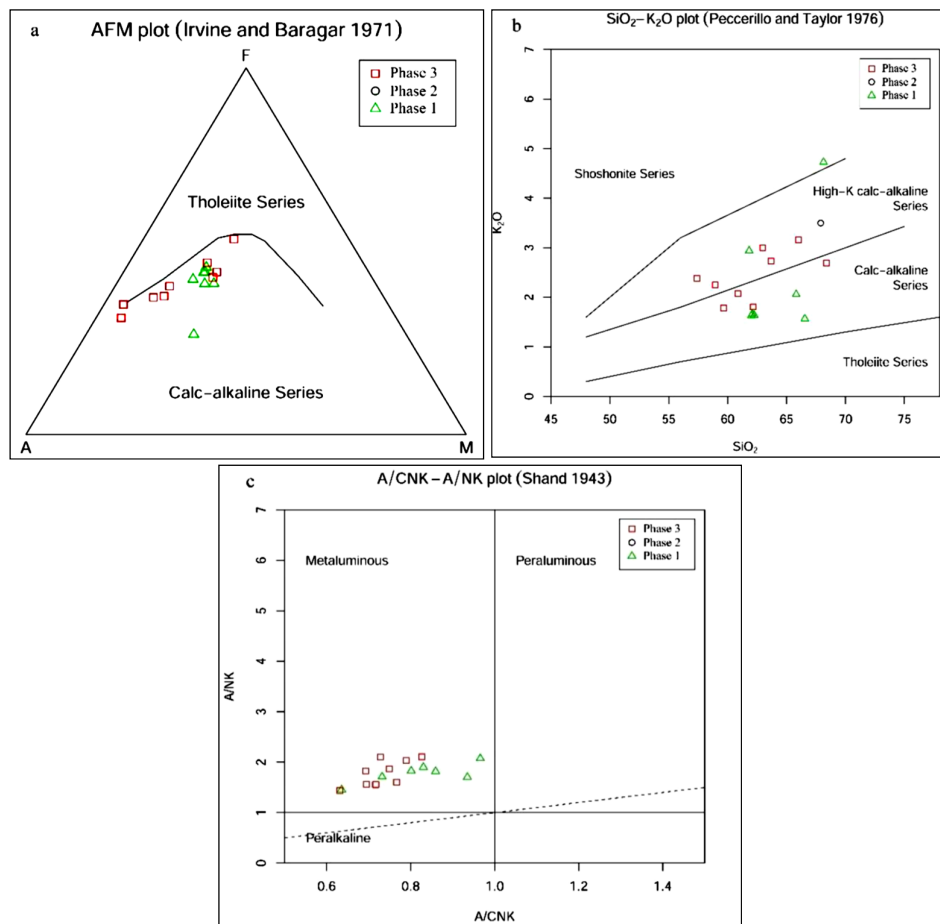


Figure 11. a) Graph of magmatic series determination of the studied volcanic rocks based on the A.F.M chart (Irvine & Baragar, 1971). b) Diagram of the magmatic series determination of volcanic rocks in the study area according to the diagram of Peccerillo & Taylor, 1976. c) The volcanic rocks diagram of the study area according to the diagram of Shand (1943)

According to the Fig. 11b (Peccerillo & Taylor, 1976), the samples of the study area are located within the calc-alkaline series and the high potassium calc-alkaline series, of which the high value of potassium based on norm and geochemical data represent magmatic fractionation and a presence of water in magma (Heidari, 2015).

In the diagram of Shand (1943), the samples of the study area are located within the metaluminous range, which is associated with the evidence of an oceanic crust subduction under the continental crust (based on the presence of Precambrian basement in the study area and composition of volcanic rocks). The feature can be seen in the northern Urmia-Dokhtar magmatic belt and the general geodynamics of Central Iran and Urmia-Dokhtar magmatic belt conforms it (Fig. 11c).

Geotectonic setting

In Zr / Ti and Zr/Ti/100/3y diagrams (Pearce & Cann, 1973) and La 10/Y15/Nb8 (Cabanis + Lecolle 1989) and TiO₂/Al₂O₃ (Muller et al., 1992), the samples of the study area are located within the range of continental arc basalts, which seems to be of post-collisional setting (Figs. 12a to 12d).

The rocks are enrichment in light rare-earth elements (LREE: La, Ce, Pr, Nd) and large ion lithophile elements (LILE: Cs, Rb, Ba, Th, U, K, Pb, Sr), but are depleted in high-field-strength elements (HFSE: Ti, Nb, Zr, P). Similar mantle pattern represents arcs with one type magma (Fig. 13a). REE patterns of the rocks are consistent with crystal fractionations (Fig. 13b).

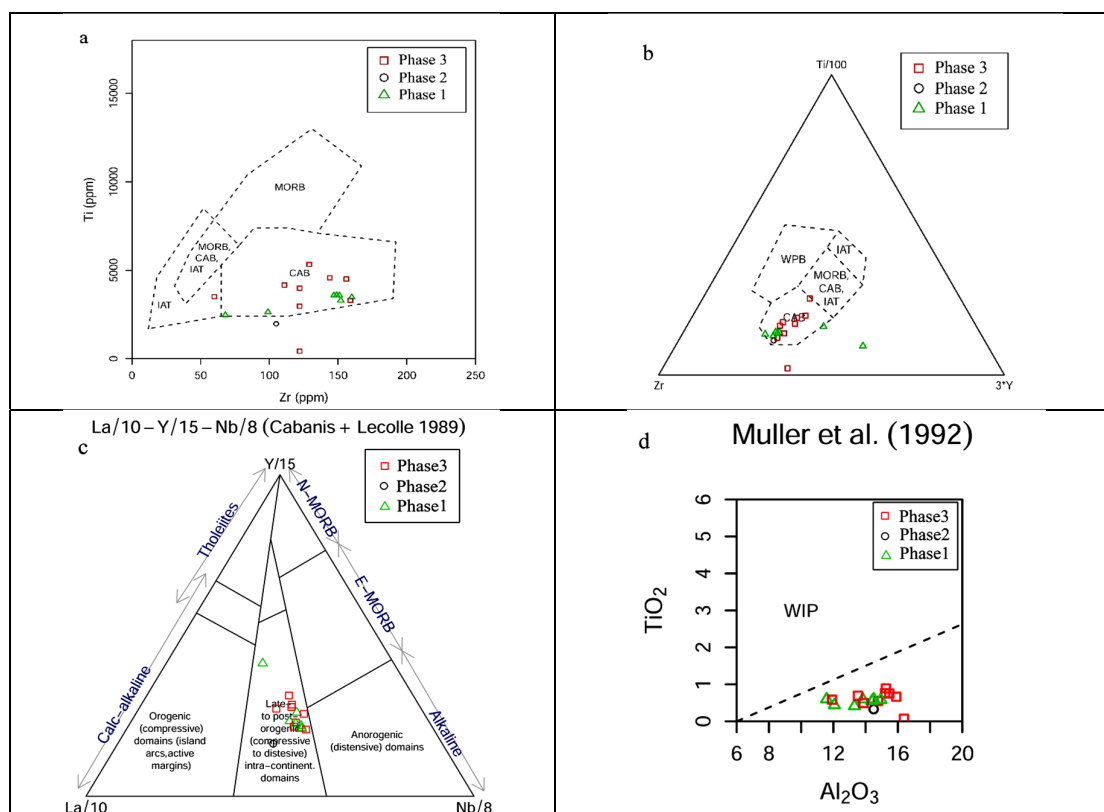


Figure 12. a) Volcanic rocks diagram of the study area according to Zr / Ti diagram (Pearce & Cann, 1973): CAB: Calc-alkali basalts; MORB, CAB, IAT: mid-ocean-ridge basalt, calc-alkali basalts, Island arc tholeiites. b) Volcanic rocks diagram of the study area according to Zr/Ti/100/3y diagram (Pearce & Cann, 1973): IAT= island-arc tholeiites; MORB= mid-ocean-ridge basalt; CAB = Continental arc basalt; WPB = within-plate basalts. c) La/10-Y/15-Nb/8 diagram (Cabanis+Lecolle, 1989). d) TiO₂ / Al₂O₃ diagram (Muller et al., 1992).

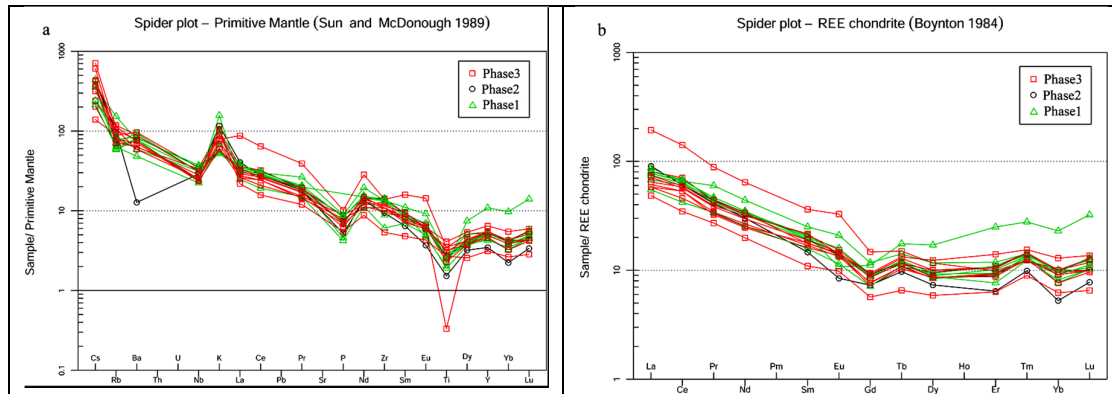


Figure 13. a) Primitive mantle spider diagram (Sun & McDonough, 1989) and b) Chondrite-REE normalized spider diagram of volcanic rocks of the study area (Boynton, 1984).

Conclusions

According to the compilation of all evidence, the field and laboratory analysis, the following results achieved:

The Eocene volcanic rocks in the studied area are very rare and the Oligo-Miocene ones are more abundant in comparison to those of other parts of Urmia-Dokhtar rocks and this feature is more evident in the Mahneshan area. They overlie the Precambrian units.

The volcanic rocks of study area can be divided into three phases.

Phase 1, hyaloclastites: They are equivalent to lower red formation. This phase has a rough and steeply dipping morphology and formed in a continental marginal environment with phreatomagmatic eruptions and caused the formation of the hyaloclastites which not reported elsewhere in Iran so far.

Phase 2, acidic tuffs of rhyodacite composition interbedded with limestone. According to the fossil content and the $^{87}\text{Sr}/^{86}\text{Sr}$ age determination, this phase formed during the Chattian to Burdigalian ages.

Phase 3, andesite-basalt and sometimes quartz-andesite which their age is mid-upper Miocene, with regard to the age of the upper and lower strata.

Among the three groups of the above-mentioned rocks, a geochemical similar affinity is commonly found, and all belong to the class of middle to high potassium calc-alkalines.

There are also differences in the nature of calc-alkaline rocks in the three groups. Phase 2 rocks are of the crustal origin and rocks of phases indicate a mantle provenance.

Geochemical evidence and regional studies show that all volcanic phases occurred in a subduction setting with a continental margin, which is consistent with the previous studies on the northern Urmia-Dokhtar magmatic belt and the evidence of the Neotethys oceanic crustal subduction under the continental crust of Central Iran.

According to Putirka (2008) equation (24a and 32d), it can be seen a synchronous formation between plagioclase and clinopyroxene of Basaltic andesite rocks from phases 1 and 3.

Plagioclase and clinopyroxene thermobarometry of basaltic andesite rocks from phases 1 and 3 show calc-alkaline series with a shallow depth that conform to presence of mineral parageneses, consisting of quartz (phase1), alkali feldspar and pyroxene (phases 1 and 3) based on petrographic studies.

According to the regional evidence and the age determination of limestones, the three magmatic phases are as follows:

-1) Hyaloclastites of Phase 1 (Oligocene), 2) Acidic tuffs of phase 2 (Late Oligocene- Early Miocene), 3) andesitic- basaltic rocks of Phase 3 (Upper Miocene).

References

- Aghanabati, A., 2004. The Geology of Iran. A Publication of the Geological Survey of Iran, Tehran, 586 p. (In Persian).
- Alavi, M., Amidi, M., 1976. Geological map of the Takab Quadrangle, West Azerbaijan Province, Iran Geological Survey & Mineral Explorations Geologic Quadrangle Map C4, Scale 1: 250000.
- Amidi, S.M., 1997. Etude geologique de la region de Natanz-Surk (Iran, Central). Ph.D thesis, Universite de Grenobl, France.
- Amidi, S.M., Emami, M.H., Michel, R., 1984. Alkaline character of Eocene volcanism in the middle part of Central Iran and its geodynamic situation, *Geologische Rundschau*, 73: 917-932.
- Asadi, H. H., Voncken, J. H. L., Kanel, R. A., Hale, M., 2000. Petrography, mineralogy and geochemistry of the Zarshuran Carlin-like gold deposit, northwest Iran, *Mineralium Deposita*, 35: 656-671.
- Berberian, M., King, G., 1981. Towards a paleogeography and tectonic evolution of Iran, *Canadian journal of earth sciences*, 18: 210-265.
- Boynnton, W.V., 1984. Cosmochemistry of the rare earth elements: meteorite studies. In: *Developments in geochemistry Elsevier*, 2: 63-114.
- Cabanis, B., Lecolle, M., 1989. Le diagramme La/10-Y/15-Nb/8; un outil pour la discrimination des series volcaniques et al mise en evidence des processus de melange et/ou de contamination crustale (The La/10-Y/15-Nb/8 diagram; a tool for distinguishing volcanic series and discovering crustal mixing and/or contamination). *Comptes Rendus de l'Academie des Sciences, Serie 2, Mecanique, Physique, Chimie, Sciences de l'Univers, Sciences de la Terre*, 309: 2023–2029.
- Caillate, C., Dehlavi, P., Martel-Jantin, B., 1978. Géologie de la région de saveh (Iran). Contribution à l'étude du volcanism et plutonisme tertiaire de la zone de l'Iran Central, These de doctorat de specialities. Universite de Grenobl, france.
- Cohen, K.M., Harper, D.A.T., Gibbard, P.L., Fan, J.-X., 2020. International Commission on Stratigraphy, January 2020.
- Daliran, F., 2008. The carbonate rock-hosted epithermal gold deposit of Agdarreh, Takab geothermal field, NW Iran-hydrothermal alteration and mineralization: *Mineralium Deposita*, 43: 383-404.
- Emami, M.H., 1991. Magmatic activity and mineral exploration. Geological Survey of Iran (In Persian).
- Ghahamghash, J., Babakhani, A., 1991. Geological map of the Takht-e Soleyman Quadrangle, West Azarbaijan Province. Iran Geological Survey & Mineral Explorations Geologic Quadrangle Map GQ-5463, Scale: 1: 100000 (In Persian).
- Ghorbani, M., 1999. Petrological investigations of tertiary-quaternary magmatic rocks and their metallogeny in Takab area. Ph.D thesis, Shahid Beheshti University (In Persian).
- Ghorbani, M., 2008. Economic Geology of Iran, Mineral Deposits and Natural Resources of Iran, A Publication of the Arain zamin (In Persian).
- Ghorbani, M., 2014. Geology of Iran. A Publication of the Arain zamin (In Persian).
- Ghorbani, M., Salehi, M., 2018. Iranology with an insight into the urban tourism, ecotourism and geotourism Vol. 4. A Publication of the Arain Zamin (In Persian).
- Heidari, M. Ghaderi, M., Afzal, P., 2013. Delineating mineralized phases based on lithogeochemical data using multifractal model in Touzlar epithermal Au-Ag (Cu) deposit, NW Iran. *Applied Geochemistry*, 31: 119-132.
- Heidari, S.M., Daliran, F., Paquette, J.L., Gasquet, D., 2015. Geology, timing, and genesis of the high sulfidation Au (-Cu) deposit of Touzlar, NW Iran, *Ore Geology Reviews*, 65: 460-486.
- Irvine, T., Baragar, W., 1971. A guide to the chemical classification of the common volcanic rocks, *Canadian journal of earth sciences*, 8: 523-548.
- Jabari, A., 2013. Petrology of volcanic and subvolcanic rocks in Kashan- Zefreh, Ph.D thesis, Shahid Beheshti University (In Persian).
- Le Bas, 1962. The role of aluminium in igneous clinopyroxenes with relation to their parentage. *American Journal of Science*, New Haven, 260: 267-288.
- Lotfi, M., 2001. Geological map of the Mahneshan Quadrangle, Zanjan Province, Iran Geological Survey & Mineral Explorations Geologic Quadrangle Map GQ-5563, Scale1: 100000 (In Persian).
- Mehrabi, B., Yardley, B., Cann, J., 1999. Sediment-hosted disseminated gold mineralisation at Zarshuran, NW Iran, *Mineralium Deposita*, 34: 673-696.

- Middlemost, E., 1985. *Magmas and magmatic rocks*. ed. London, Longman press, 266p.
- Morimoto, N., 1989. Nomenclature of pyroxenes, *Mineralogical Journal*, 14: 198-221.
- Pearce, J.A., Cann, J.R., 1973. Tectonic setting of basic volcanic rocks determined using trace element analyses, *Earth and planetary science letters*, 19: 290-300.
- Muller, D., Rock NMS., Groves DI., 1992. Geochemical discrimination between shoshonitic and potassic volcanic rocks in different tectonic setting: a pilot study. *Mineralogy and Petrology*, 46: 259-286.
- Ojaghi, B., Hoseini, M., 2005. Review of Gold genesis, Tuzlar deposit, Nw of Mahnesan, 21st Iranian Symposium of Earth Science, Iran. Tehran.
- Peccerillo, A., Taylor, S., 1976. Geochemistry of Eocene calc-alkaline volcanic rocks from the Kastamonu area, northern Turkey, *Contributions to mineralogy and petrology*, 58: 63-81.
- Pin, C., Briot, D., Bassin, C., Poitrasson, F., 1994. Concomitant separation of strontium and samarium-neodymium for isotopic analysis in silicate samples, based on specific extraction chromatography, *Analytica Chimica Acta*, 298: 209-217.
- Putirka, K.D., 2008. Thermometers and Barometers for Volcanic Systems. *Reviews in Mineralogy & Geochemistry*, 69: 61-120.
- Shand, S.J., 1943. *The eruptive rocks*. 2nd edition, John Wiley. New York, 444 p.
- Soesoo, A., 1997. A multivariate statistical analysis of clinopyroxene composition: Empirical coordinates for the crystallisation PT-estimations, *GFF*, 119: 55-60.
- Stocklin, J., 1968. Structural history and tectonics of Iran: a review, *Association of Petroleum Geologists Bulletin, USA*, 52: 1229-1258.
- Sun, S. S., McDonough, W. F., 1989. Chemical and isotopic systematics of oceanic basalts: Implications for mantle composition and processes. In: Saunders A D, Norry M J, eds. *Magmatism in the Ocean Basins*. GeolSoc London Special publication, 42: 313-345



This article is an open-access article distributed under the terms and conditions of the Creative Commons Attribution (CC-BY) license.